nature climate change

ARTICLES

https://doi.org/10.1038/s41558-018-0177-y

Forest-rainfall cascades buffer against drought across the Amazon

Arie Staal[1*], Obbe A. Tuinenburg[2], Joyce H. C. Bosmans[3], Milena Holmgren[4], Egbert H. van Nes[1], Marten Scheffer[1], Delphine Clara Zemp[5,6] and Stefan C. Dekker[2,7]

Tree transpiration in the Amazon may enhance rainfall for downwind forests. Until now it has been unclear how this cascading effect plays out across the basin. Here, we calculate local forest transpiration and the subsequent trajectories of transpired water through the atmosphere in high spatial and temporal detail. We estimate that one-third of Amazon rainfall originates within its own basin, of which two-thirds has been transpired. Forests in the southern half of the basin contribute most to the stability of other forests in this way, whereas forests in the south-western Amazon are particularly dependent on transpired-water subsidies. These forest-rainfall cascades buffer the effects of drought and reveal a mechanism by which deforestation can compromise the resilience of the Amazon forest system in the face of future climatic extremes.

The Amazon rainforest and its wet climate are mutually dependent[1–3]. Although their interactions have been a topic of study for decades[2,4–12], we still lack a deep understanding of the positive effects between forests and rainfall across the Amazon basin. Forests access groundwater in deep soil layers and release it to the atmosphere by transpiration[1,13]. This transpired moisture can precipitate and evapotranspire repeatedly over forests[14,15], promoting forest growth in a cascading way. The significance of such cascades is poorly understood due to uncertainties regarding the contribution of tree transpiration to total evapotranspiration, the atmospheric path of this transpiration to rainfall, the number of re-evapotranspiration cycles that water goes through and the effect of the resulting rainfall increase on local forest stability[3,8,16]. Also, the temporal variability of the forest's self-stabilizing mechanism is poorly understood[8]. In the wet tropics including the Amazon, tree cover declines at higher seasonal and inter-annual rainfall variability[17]. To understand the effects of extreme weather events and deforestation, a quantitative and temporally explicit assessment of the forest-rainfall cascades[18,19] is needed[8]. We can now track moisture flows quantitatively using empirically derived atmospheric wind patterns, evapotranspiration and rainfall[2,20]. Also, complex models are being improved that can quantify the contribution of vegetation to evapotranspiration on increasingly high spatial and temporal resolutions[21]. Finally, remote sensing now provides tools to quantify forest resilience[22–25]. Here, we capitalize on those technological advances to provide an empirically derived quantification of the spatial and temporal interactions between rainfall and tree cover in tropical South America, focusing on the Amazon basin (Methods). We use a Lagrangian moisture-tracking algorithm[26–28] that calculates atmospheric water flows in time steps of 0.25 h. We use output on a 0.25° grid (around 25 km × 25 km) and monthly basis for 2003–2014. We account for multiple re-evapotranspiration cycles of this moisture[15] and use a large-scale hydrological model to calculate the evapotranspiration change from potential tree-cover loss for each month[21,29]. Combined, these calculations allow us to estimate the contribution of tree cover to rainfall and related forest resilience in downwind areas. As tree transpiration is a source of atmospheric moisture that can be maintained in periods when rainfall is absent[30], we focus on the role of transpiration-induced rainfall.

We find that trees within the Amazon have transpired 20% of all rainfall in the basin at least once (Fig. 1). We call this contribution of trees to rainfall the transpiration recycling ratio (TRR). Half of this transpiration recycling occurs in a direct way, in which moisture falls back as rainfall after having last entered the atmosphere through transpiration. The other half is composed of cascading transpiration recycling (see Methods) in which transpiration-induced rainfall goes through an additional evapotranspiration–rainfall cycle at least once (Fig. 1 and Supplementary Fig. 10). Considering all evapotranspiration (including transpiration), we find that 32% of Amazonian rainfall originates from the basin, in good agreement with 10 previous estimates based on different methodologies and datasets (24–41% (median 28%); see Methods and ref. [15], including the references therein). Combining this evapotranspiration recycling with our transpiration recycling estimates, we find that 64% of all regionally recycled water has travelled through the pores of leaves of trees in the Amazon. The cascading contribution of transpiration to rainfall entails that its effects can be remote and, because a single transpired water molecule can undergo multiple re-evapotranspiration and rainfall cycles, could be larger than the transpired amount of water itself. We estimate that the largest transpiration is from the north-eastern, southern and south-western parts of the Amazon basin (Fig. 2a and Supplementary Fig. 4), in agreement with other global transpiration estimates[31,32]. Loss of tree cover in these regions would thus result in the largest loss of moisture for the basin. The small transpiration flux in the north-western Amazon is striking, but could be explained by the high moisture interception by the forest canopy[31,33] and lack of a pronounced dry season (Supplementary Fig. 3). In addition, this region has relatively low estimated potential evapotranspiration (not shown). Across the Amazon, we find little spatial difference in the distances that transpired molecules travel

[1]Aquatic Ecology and Water Quality Management Group, Wageningen University, Wageningen, The Netherlands. [2]Department of Environmental Sciences, Copernicus Institute for Sustainable Development, Utrecht University, Utrecht, The Netherlands. [3]Department of Physical Geography, Utrecht University, Utrecht, The Netherlands. [4]Resource Ecology Group, Wageningen University, Wageningen, The Netherlands. [5]Biodiversity, Macroecology and Biogeography Group, University of Goettingen, Göttingen, Germany. [6]Earth System Analysis, Potsdam Institute for Climate Impact Research, Potsdam, Germany. [7]Faculty of Management, Science and Technology, Open University, Heerlen, The Netherlands. *e-mail: ariestaal@gmail.com

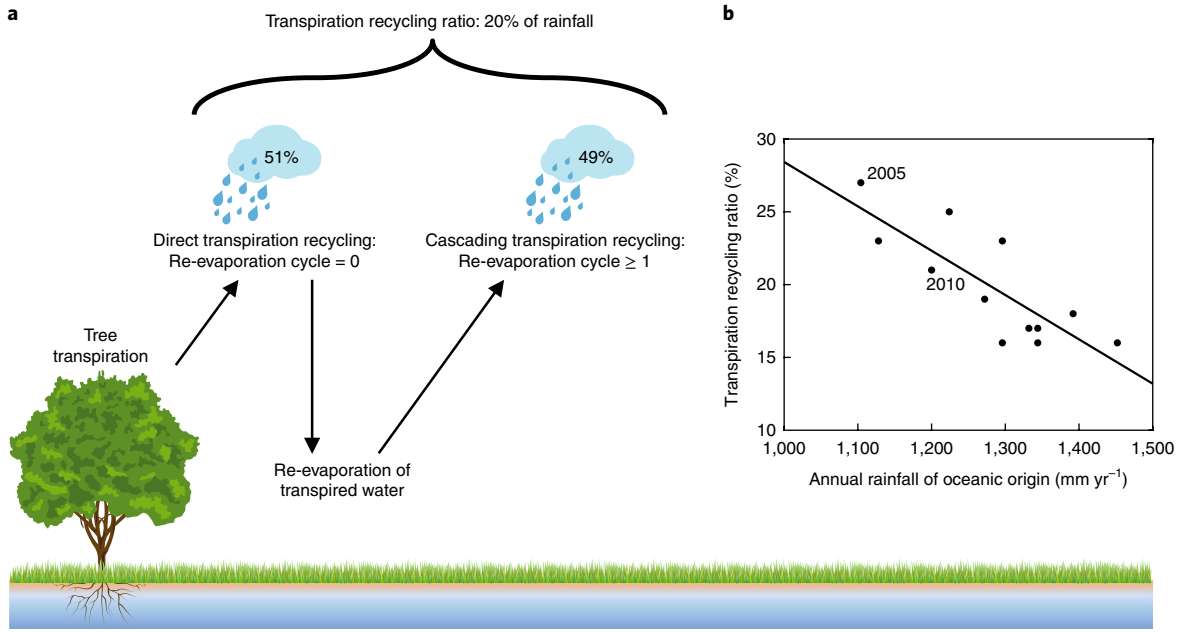

Fig. 1 | Transpiration recycling in the Amazon basin. a, On average, 20% of all rainfall in the Amazon has been transpired by trees at least once (the transpiration recycling ratio, TRR). About half of this transpiration recycling (51% of transpiration recycling) occurs after one transpiration–rainfall cycle (re-evapotranspiration cycle = 0). The remainder (49% of transpiration recycling) occurs after multiple (1–7) re-evapotranspiration cycles of transpired water (cascading transpiration recycling). **b**, Plot of the TRR in the Amazon for each year in the period 2003–2014 against the spatially averaged rainfall that had last evaporated from the ocean, *O*. A linear regression was fit, with TRR = 45 – 0.023 *O* (r^2 = 0.66). The years 2005 and 2010 are labelled because they brought drought across vast areas of the Amazon (see also Supplementary Figs. 8 and 9). See Supplementary Fig. 6 for TRRs against monthly rainfall of oceanic origin.

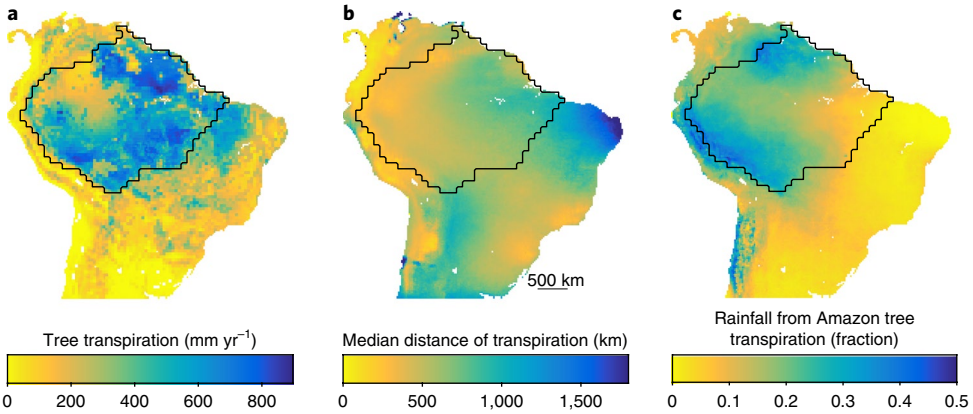

Fig. 2 | From transpiration to rainfall. a, Mean annual transpiration by trees that precipitates over land. **b**, Median geographic distance of transpired water before precipitating again over land. Distances are given at the locations of transpiration. **c**, Fraction of mean annual rainfall that has been transpired by trees in the Amazon basin. The Amazon basin is shown by a black outline.

before raining out again, with a median of ~600 km (Fig. 2b). This short distance—relative to the size of the Amazon—implies that a large part of Amazonian transpiration rains out over the basin itself: 46% of transpiration directly rains out over the Amazon (the same order of magnitude as a previous estimate based on a different methodological approach[34]). We find that if cascading recycling of that water is included, this ratio reaches 77%. The large transpiration fluxes in the Amazon (Fig. 2a) enhance rainfall over vast areas outside the basin as well (Fig. 2c).

We find temporal variations in the effect of trees on rainfall. The seasonal variability in tree-transpired rainfall is characterized by a peak during September to November, when large parts of the Amazon are at the end of the dry season, with up to 70% of regional rainfall being a result of tree transpiration (Fig. 3a–f and Supplementary Fig. 7; see Supplementary Figs. 5 and 6 for Amazon-wide monthly recycling). This large contribution of recycled moisture during the dry season means that seasonal droughts are moderated by forests. Forests also buffer against inter-annual droughts, as reflected by the negative correlation between the TRR and the amount of moisture that enters the Amazon basin (Fig. 1b). Indeed, we find the highest TRR (27%) for 2005 (Fig. 1b and Supplementary Figs. 5 and 8) during a severe drought[35]. This increased contribution of tree transpiration to rainfall could explain a previous report of relatively high moisture recycling in 2005[36]. Curiously, the contribution of tree transpiration to rainfall during the 2010 drought was lower, when the TRR remained around the multi-year average level (21%; Fig. 1b). This

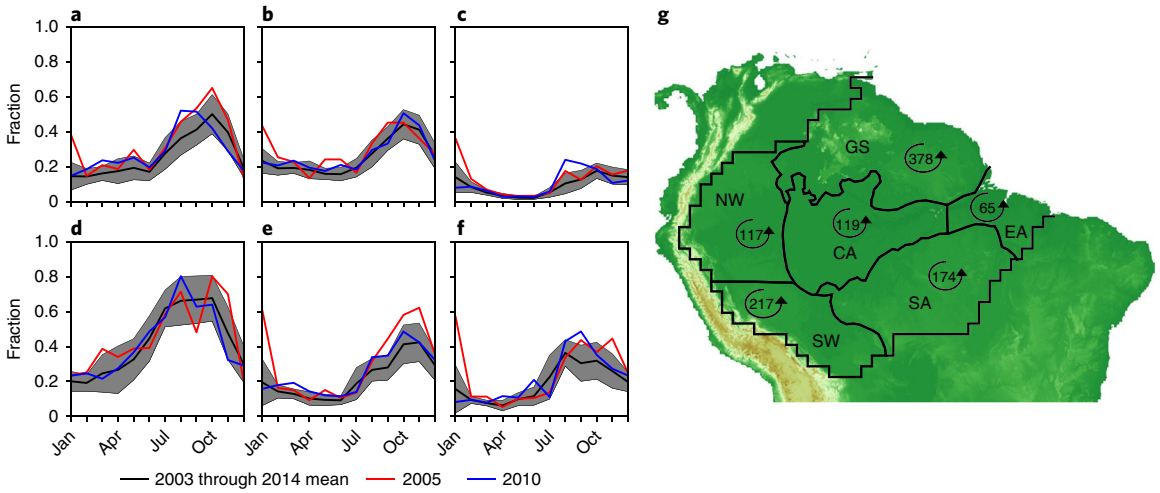

Fig. 3 | Effect of Amazonian tree transpiration on rainfall in each of the subregions of the Amazon basin. a–f, Fraction of monthly rainfall in the north-western Amazon (**a**), Guyana Shield (**b**), eastern Amazon (**c**), south-western Amazon (**d**), central Amazon (**e**) and southern Amazon (**f**) that has transpired from trees in the Amazon. The grey shaded area represents ±1 standard deviation of the mean for 2003 through 2014. **g**, Map of the six subregions[51]. The numbers inside arrows show the mean annual rainfall (in mm) that has been transpired by trees within the same subregion. Larger values imply a larger feedback of forest disturbances, such as fires, to forests within the same region. A deeper green represents lower elevation. CA, central Amazon; EA, eastern Amazon; GS, Guyana Shield; NW, north-western Amazon; SA, southern Amazon; SW, south-western Amazon.

could be explained by differences in incoming oceanic moisture. Even though large areas were affected by drought in 2010[37], we find that the total amount of oceanic moisture entering the Amazon was average (Fig. 1b and Supplementary Fig. 9). This average moisture inflow in 2010 explains its lower TRR compared with the drought of 2005, when rainfall of oceanic origin was, on average, 100 mm yr^{-1} lower than in 2010 (Fig. 1). The consistent buffering of droughts by transpiration means that the forest-rainfall cascades are at their strongest during dry periods. This is particularly relevant because both seasonal[23,38] and inter-annual rainfall variability[17] affect forest resilience in the wet tropics.

Our analysis shows that the south-western Amazon is a pronounced sink area, not just for continental moisture recycling[14,20,39] but for tree-transpired moisture in particular. This region was not only driest during 2003–2014 (Supplementary Fig. 3), but is also most dependent on locally transpired water (Fig. 3g). These results already suggest that land-cover changes in the south-western Amazon would considerably increase its vulnerability to drought, but several additional lines of evidence also indicate that forests in this region are sensitive. It has been shown that in the southern Amazon, the onset of the wet season depends on the presence of the forest[40]. In the western Amazon, the regional-scale level of photosynthetic activity requires multiple years to recover from extreme drought[41]. This is also a region where extensive floodplain forests are particularly vulnerable to fire, because they regenerate slowly or even remain under arrested succession once burnt[42]. Because fire occurrence in the Amazon increases exponentially with dry-season rainfall deficit[43], the drought-buffering capacity of the forest could greatly reduce the risk of such fires. To explore this effect, we calculated how the mean annual water deficit (see Methods) would change in the absence of forest-rainfall cascades. We find that the mean annual water deficit in the south-western Amazon would increase from 196 to 380 mm, suggesting that forest-rainfall cascades are indeed a major suppressor of forest fires in the south-western Amazon and may thus sustain a large proportion of its tree cover[3,44].

An issue of particular concern is the possibility that parts of the Amazon forest may cross a tipping point to a savannah state[18,19,44–46]. Empirical relationships between tree cover and rainfall[22,38] indicate that in South America, forest and savannah can be alternative stable states below 2,000 mm mean annual rainfall (Fig. 4). Independent evidence also indicates that below 2,000 mm rainfall, tropical forests may not maintain year-round photosynthesis[47] and may recover more slowly from perturbations when rainfall decreases[25]. This makes these forests vulnerable to die back, after which a fire-maintained savannah state may establish[38]. The strong dependence of tropical forest resilience to rainfall has also been reported for South American secondary forests[48]. We therefore used mean annual rainfall to quantify forest resilience following published methods[22] and find that resilience of the south-western Amazon forest strongly depends on forest-rainfall cascades (Fig. 4d,g; see also refs [44,49]). Without them, the rainfall regime would make savannah a much more resilient ecosystem type than forest. As Fig. 3g showed, much of the tree-induced rainfall in the south-western Amazon has been transpired nearby. This implies that forest disturbances that affect transpiration feed back to forests in the same region, further amplifying these disturbances. Thus, it is important to understand how climate change and deforestation alter transpiration and wind patterns[50], as consequences for the south-western Amazon may be large. Forests in the northern part of the basin (for example, the north-western Amazon and Guyana Shield) are also relatively dependent on forest-rainfall cascades and are at risk of tipping to a savannah state, but this dependency is spatially less extensive than in the south-west (Fig. 4g).

Having determined how rainfall changes would affect forest resilience in each 0.25° cell, we weighted all transpiration fluxes by their effect on resilience across the Amazon (Methods). We then aggregated these positive effects of transpiration on resilience and ranked all 0.25° cells accordingly. In line with the results from a recent modelling study[49], we found a marked north–south gradient in the contribution of tree transpiration to forest resilience (Fig. 5). This can be explained by the relatively large prevalence of dry conditions (low mean annual rainfall and a longer dry season between June and September) towards the south (Supplementary Fig. 3), which increases tree transpiration (Fig. 2a) and the contribution of transpired water to rainfall (Supplementary Fig. 7), and decreases forest resilience[22]. Furthermore, in the dry season the dominant wind pattern in the southern Amazon is westward rather than southward[15], enhancing transpired moisture retention in the basin compared with the wet season (December to March).

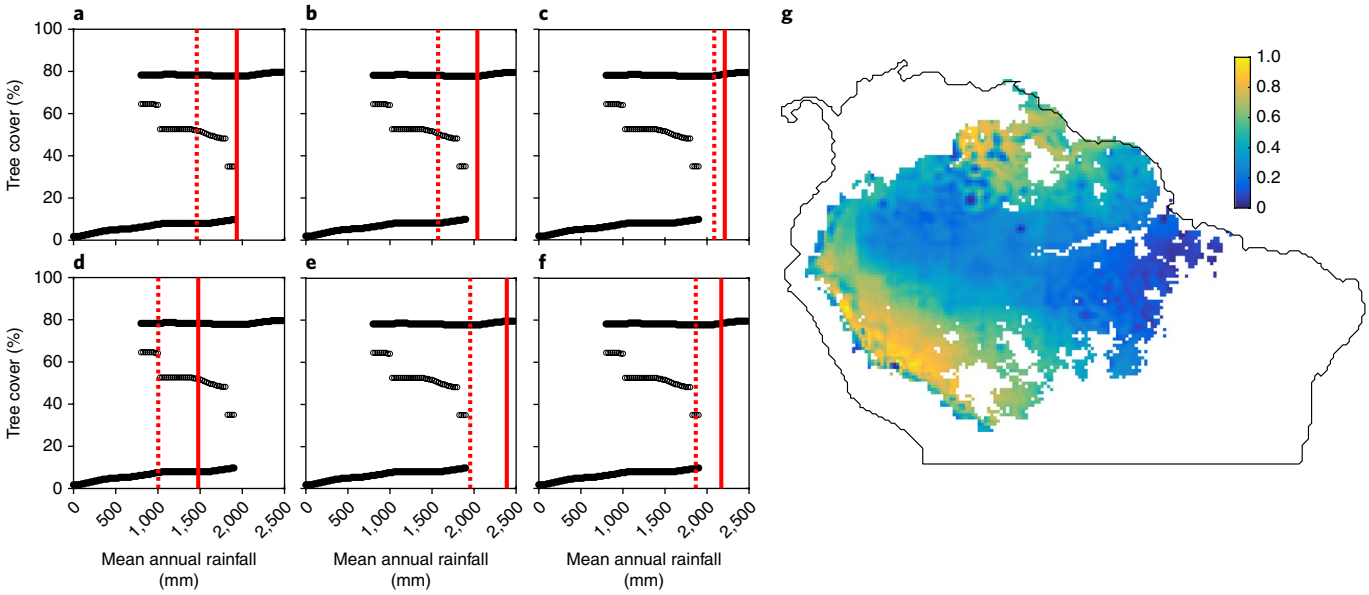

Fig. 4 | Effect of Amazon tree transpiration on Amazon forest resilience. a–f, Mean annual rainfall for 2003–2014 with (solid red line) and without (dotted red line) the contribution of transpiration from Amazonian tree cover for the north-western Amazon (**a**), Guyana Shield (**b**), eastern Amazon (**c**), south-western Amazon (**d**), central Amazon (**e**) and southern Amazon (**f**). The black lines show an empirically constructed hysteresis plot of tree cover against the mean annual rainfall for South American forests. **g**, Resilience loss for Amazonian forests, quantified as the fraction of resilience (as defined previously[22] (see Methods)) that would be lost in the absence of tree transpiration by Amazonian trees.

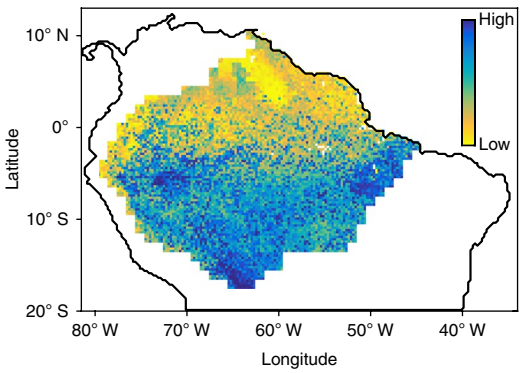

Fig. 5 | All 0.25° cells in the Amazon basin ranked by their contribution to Amazonian forest resilience through tree transpiration. Blue indicates a high contribution and yellow a low contribution. This contribution depends on the transpiration from trees in the source, the sink areas to which this transpired water flows, and the rainfall regime and tree cover in these sink areas. Hence, this ranking should be interpreted as the contribution of an area's trees to Amazon forest-rainfall cascades.

The importance of southern Amazon forests as a source of moisture coincides with their risk of being deforested. Historically, deforestation has been concentrated in the south of the basin. Indeed, we find that if twenty-first-century deforestation had not occurred, the TRR would have been 24% instead of 20%. For a business-as-usual deforestation scenario (Supplementary Fig. 12), the estimated TRR is predicted to drop to 16% by 2050 (assuming rainfall and atmospheric patterns of 2003–2014; see Methods). Our results imply that neglection of forest-rainfall cascades would result in substantial underestimation of the ecosystem services delivered by the Amazon rainforest.

Methods

Methods, including statements of data availability and any associated accession codes and references, are available at https://doi.org/10.1038/s41558-018-0177-y.

Received: 24 May 2017; Accepted: 25 April 2018;
Published online: 28 May 2018

References

1. Aragão, L. E. O. C. The rainforest's water pump. *Nature* **489**, 217–218 (2012).
2. Spracklen, D. V., Arnold, S. R. & Taylor, C. Observations of increased tropical rainfall preceded by air passage over forests. *Nature* **489**, 282–285 (2012).
3. Zemp, D. C. et al. Self-amplified Amazon forest loss due to vegetation–atmosphere feedbacks. *Nat. Commun.* **8**, 14681 (2017).
4. Costa, M. H. & Foley, J. A. Water balance of the Amazon basin: dependence on vegetation cover and canopy conductance. *J. Geophys. Res. Atmos.* **102**, 23973–23989 (1997).
5. Costa, M. H. & Pires, G. F. Effects of Amazon and central Brazil deforestation scenarios on the duration of the dry season in the arc of deforestation. *Int. J. Climatol.* **30**, 1970–1979 (2010).
6. Davidson, E. A. et al. The Amazon basin in transition. *Nature* **481**, 321–328 (2012).
7. Malhi, Y. et al. Climate change, deforestation, and the fate of the Amazon. *Science* **319**, 169–172 (2008).
8. Nobre, C. A. et al. Land-use and climate change risks in the Amazon and the need of a novel sustainable development paradigm. *Proc. Natl Acad. Sci. USA* **113**, 10759–10768 (2016).
9. Nobre, C. A., Sellers, P. J. & Shukla, J. Amazonian deforestation and regional climate change. *J. Clim.* **4**, 957–988 (1991).
10. Oyama, M. D. & Nobre, C. A. A new climate–vegetation equilibrium state for tropical South America. *Geophys. Res. Lett.* **30**, 2199 (2003).
11. Sampaio, G. et al. Regional climate change over eastern Amazonia caused by pasture and soybean cropland expansion. *Geophys. Res. Lett.* **34**, L17709 (2007).
12. Bagley, J. E., Desai, A. R., Harding, K. J., Snyder, P. K. & Foley, J. A. Drought and deforestation: has land cover change influenced recent precipitation extremes in the Amazon? *J. Clim.* **27**, 345–361 (2014).
13. Nepstad, D. C. et al. The role of deep roots in the hydrological and carbon cycles of Amazonian forests and pastures. *Nature* **372**, 666–669 (1994).
14. Eltahir, E. A. B. & Bras, R. L. Precipitation recycling in the Amazon basin. *Q. J. R. Meteorol. Soc.* **120**, 861–880 (1994).
15. Zemp, D. C. et al. On the importance of cascading moisture recycling in South America. *Atmos. Chem. Phys.* **14**, 13337–13359 (2014).
16. Fisher, J. B. et al. The future of evapotranspiration: global requirements for ecosystem functioning, carbon and climate feedbacks, agricultural management, and water resources. *Water Resour. Res.* **53**, 2618–2626 (2017).
17. Holmgren, M., Hirota, M., van Nes, E. H. & Scheffer, M. Effects of interannual climate variability on tropical tree cover. *Nat. Clim. Change* **3**, 755–758 (2013).

18. Malhi, Y. et al. Exploring the likelihood and mechanism of a climate-change-induced dieback of the Amazon rainforest. *Proc. Natl Acad. Sci. USA* **106**, 20610–20615 (2009).
19. Nepstad, D. C., Stickler, C. M., Soares-Filho, B. & Merry, F. Interactions among Amazon land use, forests and climate: prospects for a near-term forest tipping point. *Phil. Trans. R. Soc. Lond. B Biol. Sci.* **363**, 1737–1746 (2008).
20. Van der Ent, R. J., Savenije, H. H. G., Schaefli, B. & Steele-Dunne, S. C. Origin and fate of atmospheric moisture over continents. *Water Resour. Res.* **46**, W09525 (2010).
21. Van Beek, L. P. H., Wada, Y. & Bierkens, M. F. P. Global monthly water stress: 1. Water balance and water availabilty. *Water Resour. Res.* **47**, W07517 (2011).
22. Hirota, M., Holmgren, M., van Nes, E. H. & Scheffer, M. Global resilience of tropical forest and savanna to critical transitions. *Science* **334**, 232–235 (2011).
23. Staal, A., Dekker, S. C., Xu, C. & van Nes, E. H. Bistability, spatial interaction, and the distribution of tropical forests and savannas. *Ecosystems* **19**, 1080–1091 (2016).
24. Xu, C. et al. Remotely sensed canopy height reveals three pantropical ecosystem states. *Ecology* **97**, 2518–2521 (2016).
25. Verbesselt, J. et al. Remotely sensed resilience of tropical forests. *Nat. Clim. Change* **6**, 1028–1031 (2016).
26. Dirmeyer, P. A. & Brubaker, K. L. Contrasting evaporative moisture sources during the drought of 1988 and the flood of 1993. *J. Geophys. Res. Atmos.* **104**, 19383–19397 (1999).
27. Dirmeyer, P. A. & Brubaker, K. L. Characterization of the global hydrologic cycle from a back-trajectory analysis of atmospheric water vapor. *J. Hydrometeorol.* **8**, 20–37 (2007).
28. Tuinenburg, O. A., Hutjes, R. W. A. & Kabat, P. The fate of evaporated water from the Ganges basin. *J. Geophys. Res. Atmos.* **117**, D01107 (2012).
29. Bosmans, J. H. C., van Beek, L. P. H., Sutanudjaja, E. H. & Bierkens, M. F. P. Hydrological impacts of global land cover change and human water use. *Hydrol. Earth Syst. Sci.* **21**, 5603–5626 (2017).
30. Von Randow, C. et al. Comparative measurements and seasonal variations in energy and carbon exchange over forest and pasture in South West Amazonia. *Theor. Appl. Climatol.* **78**, 5–26 (2004).
31. Wang-Erlandsson, L., van der Ent, R. J., Gordon, L. J. & Savenije, H. H. G. Contrasting roles of interception and transpiration in the hydrological cycle—part 1: temporal characteristics over land. *Earth Syst. Dynam.* **5**, 441–469 (2014).
32. Miralles, D. G. et al. The WACMOS-ET project—part 2: evaluation of global terrestrial evaporation data sets. *Hydrol. Earth Syst. Sci.* **20**, 823–842 (2016).
33. Miralles, D. G., Gash, J. H., Holmes, T. R. H., de Jeu, R. A. M. & Dolman, A. J. Global canopy interception from satellite observations. *J. Geophys. Res. Atmos.* **115**, D16122 (2010).
34. Van der Ent, R. J., Wang-Erlandsson, L., Keys, P. W. & Savenije, H. H. G. Contrasting roles of interception and transpiration in the hydrological cycle—part 2: moisture recycling. *Earth Syst. Dynam.* **5**, 471–489 (2014).
35. Zeng, N. et al. Causes and impacts of the 2005 Amazon drought. *Environ. Res. Lett.* **3**, 014002 (2008).
36. Satyamurty, P., da Costa, C. P. W. & Manzi, A. O. Moisture source for the Amazon basin: a study of contrasting years. *Theor. Appl. Climatol.* **111**, 195–209 (2013).
37. Lewis, S. L., Brando, P. M., Phillips, O. L., van der Heijden, G. M. F. & Nepstad, D. The 2010 Amazon drought. *Science* **331**, 554 (2011).
38. Staver, A. C., Archibald, S. & Levin, S. A. The global extent and determinants of savanna and forest as alternative biome states. *Science* **334**, 230–232 (2011).
39. Burde, G. I., Gandush, C. & Bayarjargal, Y. Bulk recycling models with incomplete vertical mixing. Part II: precipitation recycling in the Amazon basin. *J. Clim.* **19**, 1473–1489 (2006).
40. Wright, J. S. et al. Rainforest-initiated wet season onset over the southern Amazon. *Proc. Natl Acad. Sci. USA* **114**, 8481–8486 (2017).
41. Maeda, E. E., Kim, H., Aragão, L. E., Famiglietti, J. S. & Oki, T. Disruption of hydroecological equilibrium in southwest Amazon mediated by drought. *Geophys. Res. Lett.* **42**, 7546–7553 (2015).
42. Flores, B. M. et al. Floodplains as an Achilles' heel of Amazonian forest resilience. *Proc. Natl Acad. Sci. USA* **114**, 4442–4446 (2017).
43. Aragão, L. E. O. C. et al. Interactions between rainfall, deforestation and fires during recent years in the Brazilian Amazonia. *Phil. Trans. R. Soc. Lond. B* **363**, 1779–1785 (2008).
44. Pires, G. F. & Costa, M. H. Deforestation causes different subregional effects on the Amazon bioclimatic equilibrium. *Geophys. Res. Lett.* **40**, 3618–3623 (2013).
45. Lenton, T. M. et al. Tipping elements in the Earth's climate system. *Proc. Natl Acad. Sci. USA* **105**, 1786–1793 (2008).
46. Nobre, C. A. & Borma, L. D. S. 'Tipping points' for the Amazon forest. *Curr. Opin. Environ. Sustain.* **1**, 28–36 (2009).
47. Guan, K. et al. Photosynthetic seasonality of global tropical forests constrained by hydroclimate. *Nat. Geosci.* **8**, 284–289 (2015).
48. Poorter, L. et al. Biomass resilience of neotropical secondary forests. *Nature* **530**, 211–214 (2016).
49. Zemp, D. C., Schleussner, C. F., Barbosa, H. M. J. & Rammig, A. Deforestation effects on Amazon forest resilience. *Geophys. Res. Lett.* **44**, 6182–6190 (2017).
50. Khanna, J., Medvigy, D., Fueglistaler, S. & Walko, R. Regional dry-season climate changes due to three decades of Amazonian deforestation. *Nat. Clim. Change* **7**, 200–204 (2017).
51. Ter Steege, H. et al. Hyperdominance in the Amazonian tree flora. *Science* **342**, 1243092 (2013).

Acknowledgements

We thank C. Xu and H. ter Steege for providing data files. A.S. thanks S. Bathiany and B. M. Flores for useful discussions. A.S. was supported by a PhD scholarship from SENSE Research School. O.A.T. was supported by the Netherlands Organization for Scientific Research under the Innovational Research Incentives Scheme Veni (grant agreement 016.171.019). E.H.v.N. and M.S. were supported by the European Union's Horizon 2020 research and innovation programme under Marie Skłodowska-Curie grant agreement 643073 (ITN CRITICS). D.C.Z. was supported by IRTG 1740/TRP 2011/50151-0, funded by the DFG and FAPESP. This work was carried out under the programme of the Netherlands Earth System Science Centre.

Author contributions

A.S., O.A.T. and S.C.D. designed the research. A.S., O.A.T. and J.H.C.B. carried out the analyses. All authors interpreted the results. A.S. wrote the paper with contributions from all authors.

Competing interests

The authors declare no competing interests.

Additional information

Supplementary information is available for this paper at https://doi.org/10.1038/s41558-018-0177-y.

Reprints and permissions information is available at www.nature.com/reprints.

Correspondence and requests for materials should be addressed to A.S.

Publisher's note: Springer Nature remains neutral with regard to jurisdictional claims in published maps and institutional affiliations.

Methods

Study region and period. We performed simulations for all of tropical South America (13° N–35° S). Thus, moisture that leaves the Amazon basin through the atmosphere and subsequently re-enters it is accounted for in the results. Our definition of the Amazon basin includes the Guyana Shield, following ref. [51]. We divided the basin into six subregions for Figs. 3 and 4, also following ref. [51], which adapted the division by refs [52,53] based on soil distributions in the Amazon. Our study period covers 2003–2014 and we present output on 0.25° resolution (around 25 km × 25 km).

Quantifying tree transpiration. We performed spatially and temporally explicit calculations of the contribution of tree cover to evapotranspiration. Thus, transpiration from all types of tree cover, including savannahs, is involved in these estimates of tree transpiration. For our calculations, we applied the PCRaster Global Water Balance hydrological model (PCR-GLOBWB) at 0.5° resolution. PCR-GLOBWB is a hydrological and water resources model that computes the vertical water balance in two soil layers (the upper one being a maximum of 30 cm and the lower one a maximum of 120 cm) and a groundwater layer. Roots deeper than 150 cm have been reported for the Amazon[54], implying that we might underestimate dry-season transpiration. Water can be stored in the canopy, snow, soil, rivers, lakes and groundwater. Sub-grid variability is taken into account by including the soil-type distribution (FAO Digital Soil Map of the World), fractional area of saturated soil[55] and spatiotemporal distribution of groundwater depth based on the groundwater storage and the surface elevations. More detailed model descriptions can be found in earlier studies[29,56]. However, we take into account transpiration from only natural tree cover, which include the 'natural vegetation' land-cover types with a forest fraction in the Global Land Cover Characterization dataset[57].

We forced the model with WATCH Forcing Data ERA-Interim temperature, precipitation and reference potential evapotranspiration[58]. Reference potential evapotranspiration was computed using the FAO Penman–Monteith equation[59]. In some cells in months with very little evapotranspiration, tree transpiration in PCR-GLOBWB could be greater than evapotranspiration in the Global Land Data Assimilation System (GLDAS) dataset used for atmospheric moisture tracking (see below). In these cases, we set tree transpiration at evapotranspiration.

For each simulated year, we excluded the cumulative deforestation up to the year before. For this, we aggregated the annual reported deforestation in the PRODES (Projeto de Monitoramento do Desmatamento na Amazônia Legal por Satélite) dataset provided by the Brazilian government. For each 0.25° cell, we calculated the fractional cumulative deforestation and subtracted it from the fractional tree-cover area in the land-cover distribution dataset in PCR-GLOBWB[29].

Our model has a monthly output, so in our calculations we assumed that the fraction of evapotranspiration transpired by trees remains the same for one month at a time. In the model output, tree transpiration in the Amazon is on average 45 mm month^{-1} (Supplementary Fig. 1). In line with observations[30,60], this flux decreases with increasing monthly rainfall values because rainfall is negatively correlated with incoming radiation, and because canopy interception evaporation increases with rainfall. However, total evapotranspiration from closed canopies depends only weakly on rainfall (Supplementary Fig. 1). This supports our implicit assumption that if rainfall decreases due to upwind tree-cover loss, the partitioning of rainfall over evapotranspiration, runoff and water storage remains equal.

Atmospheric moisture-tracking scheme. To estimate the atmospheric transport of transpired water, we used a water trajectory model[26–28], which tracks parcels of moisture that are released on random locations within each 0.25° cell and every 0.25 simulated hours for the period 2003–2014. Thus, this part of the calculation runs on a higher temporal and spatial resolution than the output of the PCR-GLOBWB hydrological model. This means that we had to assume that the fraction of evapotranspiration that was transpired by trees was the same within blocks of 2 × 2 cells of 0.25° for each month. The atmospheric moisture-tracking method assumes that evapotranspired water vapour is distributed over the vertical water column in the same way as the already present water vapour. Hence, a given water molecule is assigned a random starting height scaled with the humidity profile. The trajectories in time and space of these molecules are then forced by the three-dimensional ERA-Interim reanalysis estimates of wind speed and direction with a resolution of 0.75° and 6 h[61], but linearly interpolated so that the locations of parcels are updated at every time step of 0.25 h. We assume that at every time step each water molecule in the atmospheric column has equal probability of raining out. For these atmospheric fields, we used data between 1,000 and 500 hPa with a vertical resolution of 50 hPa. The amount of rainfall, A (mm), at a given location x,y and time step t that has evapotranspired from any source location in any cell is given by equation (1)[28]:

$$A_{x,y,t} = P_{x,y,t}\frac{W_{\text{parcel},t}E_{\text{source},t}}{\text{TPW}_{x,y,t}} \quad (1)$$

where P is rainfall (mm), W_{parcel} is the amount of water in the tracked parcel (mm), E_{source} (–) is the fraction of water in the parcel that evapotranspired from the source and TPW is the total precipitable water in the atmospheric water column (mm). At every time step, the amount of water in the parcel is updated based on evapotranspiration into the parcel and rainfall P out of it:

$$W_{\text{parcel},t} = W_{\text{parcel},t-1} + (\text{ET}_{x,y,t} - P_{x,y,t})\frac{W_{\text{parcel},t-1}}{\text{TPW}_{x,y,t}} \quad (2)$$

The fraction of water in the parcel that has evapotranspired from the source is then updated as:

$$E_{\text{source},t} = \frac{E_{\text{source},t-1}W_{\text{parcel},t-1} - A_{x,y,t}}{W_{\text{parcel},t}} \quad (3)$$

Thus, the amount of water that was tracked from the source decreases with precipitation along its trajectory and each parcel was followed until either less than 5% of its original amount was left in the atmosphere, the tracking time was more than 30 days or it left the study domain of 81.5° W–34° W and 13° N–35° S. Three-hourly evapotranspiration and rainfall estimates for each 0.25° cell were taken from the GLDAS2 dataset (GLDAS Noah Land Surface Model L4 3 hourly, 0.25° × 0.25°, version 2.0)[62]. Over all land points, this evapotranspiration is linearly interpolated to every 0.25 h time step. Over water bodies, there is no GLDAS estimate of evaporation, so the moisture-tracking scheme uses 6-hourly ERA-Interim evaporation at 0.75° × 0.75°, which is also linearly interpolated to every 0.25 h time step. To obtain the contribution to rainfall of evaporation from the ocean, we performed the simulation back in time so that rainfall from the sink was tracked back to the source. The moisture flow m_{ij} (mm) linking evapotranspiration in cell i to rainfall in cell j where $[x,y]\epsilon j$ over the course of a given month becomes:

$$m_{ij} = \sum_{t=0}^{\text{month}} A_{j,t}\frac{\text{ET}_{i,t}}{W_{i,t}} \quad (4)$$

where $\text{ET}_{i,t}$ is the evapotranspiration (mm) and $W_{i,t}$ is the tracked amount of water from source cell i at time step t. We performed these simulations for each month in the period 2003–2014; for each of these months, we thus obtained a dataset of moisture flows between each pair of 0.25° cells in the study domain.

We further assumed that when evapotranspiration changes, the partitioning of this water over its sink regions is unchanged. This means that we assumed that changes in forest structure do not affect the large-scale wind patterns that are relevant for moisture recycling, although the spatial pattern of deforestation affects rainfall on local-to-regional scales[50,63] and reduced transpiration could suppress oceanic moisture inflow through a reduction of latent heat releasing moisture condensation in the atmosphere[64].

Transpiration recycling. The monthly contribution of transpiration T from cell i in a source area of interest, Ω, to rainfall P in sink cell j after $n=0$ re-evapotranspiration cycles is:

$$\rho_{\Omega,j} = \sum_{i\in\Omega}\frac{m_{ij}\cdot\frac{T_i}{\text{ET}_i}}{P_j} \quad \text{if } n=0 \quad (5)$$

where $\rho_{\Omega,j}$ is the fraction of rainfall in j transpired from trees in source area Ω, $m_{i,j}$ is the moisture flow (mm month^{-1}) from cell i to cell j, T_i is the tree transpiration in cell i (mm month^{-1}) and P_j is the rainfall in cell j (mm month^{-1}). Our calculation of the contribution to rainfall by tree transpiration after n re-evapotranspiration cycles (transpiration recycling) is based on a previous study on 'cascading moisture recycling'[15]:

$$\rho^{(n)}_{\Omega,j} = \frac{\sum m_{ij}\cdot\rho^{(n-1)}_{\Omega,i}}{P_j} \quad \text{if } n>0 \quad (6)$$

A molecule of water can be transpired multiple times during its course over the continent. Summing all contributions of tree transpiration to rainfall in a given location could cause this contribution to become larger than the rainfall that directly originates from land. Therefore, we truncated the maximum contribution of transpiration to total monthly rainfall after n re-evapotranspiration cycles at the fraction of rainfall directly evapotranspired from land as follows:

$$\rho^{(n)}_{\Omega,j} = \min\left[\rho^{(n)}_{\Omega,j}, \left(1-\rho^{(0)}_{\text{ocean},j} - \sum_{k=0}^{n-1}\rho^{(k)}_{\Omega,j}\right)\right] \quad (7)$$

After six re-evapotranspiration cycles, the contribution of tree transpiration had decreased to practically zero, but we performed a seventh round as well. All results shown include the direct effect of tree-cover transpiration and the seven re-evapotranspiration cycles.

Sensitivity analyses and validations. The main assumptions of the moisture tracking scheme are that (1) the altitude at which evapotranspiration is released

into the atmospheric column scales with the humidity profile, (2) sub-grid wind speed variability (for example, due to convection[65]) is ignored and (3) there is equal chance of raining out for moisture at all altitudes in the atmospheric column. Here, we present an analysis of the sensitivity of moisture recycling to these assumptions, for which we did some additional forward moisture-tracking simulations.

In the 'low_release' simulation, the moisture is released 50 hPa (about 500 m) above the land surface. In the 'conv_transport' simulation, we use the (three-dimensional) ERA-Interim convective up- and downdraughts to stochastically displace the moisture particles vertically during the tracking. During every time step of the transport, a random number between 0 and 1 is picked. If this number is smaller than the ratio between the updraught mass flux ($M_{\mathrm{updraught}}$ (kg h^{-1} m^{-2})) over the time period δt and the mass of the atmospheric layer in the 50 hPa above the parcel (M_{layer} (kg m^{-2})), $\frac{M_{\mathrm{updraught}}\delta t}{M_{\mathrm{layer}}}$, the particle is displaced 50 hPa upwards. This 50 hPa thickness of the layer is chosen because the forcing data of mass fluxes of the updraughts and downdraughts are used at the same 50 hPa vertical resolution as the other atmospheric variables. At every time step, this procedure is repeated independently for downdraughts.

In the 'moisture_rainout' and 'condensation_rainout' simulations, the precipitation of moisture during the trajectory is not assumed to be independent of the altitude of the parcel, but is weighted with the local humidity profile and the local precipitation generation profile. The local precipitation generation profile is derived from the local precipitation flux profile, for which the data are used at the same vertical 50 hPa resolution as the wind fields. For each of these levels, the precipitation flux at 50 hPa below this level is subtracted to determine the precipitation generation between these levels.

These sensitivity tests simulate the evapotranspiration from the six Amazonian subregions (Fig. 3g) for 2003–2014. For each of these subregions, Supplementary Table 1 presents the difference in annual mean rainfall that originates from evapotranspiration in the same region relative to the 'standard' run. The altitude at which the moisture parcels are released has the largest influence on moisture recycling. When the parcels are released close to the land surface ('low_release' simulation), they stay closer to their source location (that is, where evapotranspiration occurred) and moisture recycling within the region increases substantially, except for the south-western Amazon, where recycling decreases.

Including the convective mass fluxes during transport decreases moisture recycling, as some parcels are transported higher up in the atmosphere, where wind speeds are typically higher and further away from the source location. As shown previously[65], including these convective movements in the transport can have large moisture recycling effects on individual days. However, the effect during the total period considered in this study is smaller than that of the release height. Modifying the rainout assumptions, as in the 'moisture_rainout' and 'condensation_rainout' simulations, causes a slight increase in moisture recycling.

Compared with the 'standard' simulation, the sensitivity experiments typically show larger moisture recycling, especially in regions with large vertical variability in wind directions, as found previously[66]. Given the results of these moisture-tracking sensitivity experiments, the moisture recycling rates in this study might be conservative.

There are no independent datasets on which to validate our estimates of monthly tree transpiration. However, there are estimates of total evapotranspiration. To approach a validation of our transpiration estimates for the Amazon, we relate the monthly evapotranspiration from our model PCR-GLOBWB to synthesized observation- and model-based estimates of evapotranspiration in months with relatively high contributions of transpiration to evapotranspiration. We therefore relate the datasets for dry months (that is, with rainfall below 100 mm) as well as for months where PCR-GLOBWB estimates that tree transpiration comprises at least 50% of total evapotranspiration. We used LandFlux-EVAL merged synthesis products for the period 1989–2005[67]. The 'diagnostic' dataset merges five observation-based (mainly from satellites) global datasets for evapotranspiration and the 'LSM' dataset merges estimates from five land surface models. Their spatial resolution is 1°, so we averaged all four 0.5° monthly estimates from PCR-GLOBWB in each 1° cell. PCR-GLOBWB runs are available for the total period that the LandFlux-EVAL data span. The results are shown in Supplementary Fig. 2. Our estimates of evapotranspiration correspond well with each of the four subsets, given that the r^2 values of the linear regressions all lie between 0.21 and 0.35.

We tested the sensitivity of transpiration recycling to different estimates for the transpiration fluxes. For this, we simulated transpiration recycling assuming that transpiration would consistently be −25, −10, +10 and +25% relative to our calculations. Our results were shown to be robust against these changes: in the rather extreme cases that transpiration would in reality be 25% smaller or greater than our estimates, the TRRs would be 16 or 24% (Supplementary Fig. 5). More realistic deviations of 10% from our estimates result in TRRs of 18 and 22%.

A number of previous studies estimated the evapotranspiration recycling ratio for the Amazon. This ratio does not account for transpiration specifically, but does provide possibilities to compare our estimates of recycling with those in the literature. Our estimated evapotranspiration recycling ratio for the Amazon basin is 32%. This is based on evapotranspiration estimates that already include effects of historical deforestation. Our estimate of 32% is within the range reported by earlier studies. Reported estimates range from 24 to 41%[15,39,68], with most being in the range 25–35%[14,15,20,36,39,69–71].

Forest–savannah bistability, resilience estimates and resilience-weighted transpiration. We used potential analysis[22,72] to empirically construct the hysteresis plot for forest and savannah from the probability densities of MODIS VCF5 tree-cover data on 250 m resolution[73]. We excluded human-used areas, water bodies and bare ground using the 2009 European Space Agency Globcover dataset at 300 m resolution (values 11–30 and ≥190). We took a sample of 0.1% of the continental tree-cover data points. Forest resilience R_{F} was calculated as the probability of forest (tree cover ≥50%) at a given climate by performing a logistic regression on mean annual rainfall[22] using the MATLAB function glmfit. Residual resilience R_{R} in the absence of tree transpiration was calculated with the same equation, but with the contribution of transpiration deducted from the mean annual rainfall (Supplementary Fig. 11). Loss of resilience (Fig. 4a) was quantified as $\frac{R_{\mathrm{F}}-R_{\mathrm{R}}}{R_{\mathrm{F}}}$. For the results presented in the main text, we used the GLDAS data from 2003–2014; however, because this is a short climatic period on which to base forest resilience, we also present in Supplementary Fig. 11 calculations using Climate Research Unit rainfall data on 0.5° resolution for 1961–2001[74].

We used the estimates of resilience of the sink locations to weight the transpiration from the source for its importance for Amazon forest resilience. The weighted transpiration flux of a cell i, $T_{i,\mathrm{weighted}}$, accounting for all seven re-evapotranspiration cycles, is calculated as:

$$T_{i,\mathrm{weighted}} = \sum_{k=0}^{n} \sum_{j\in\mathrm{Amazon}} m_{ij}^{k}(1-R_{\mathrm{F},j})F_j \qquad (8)$$

where $R_{\mathrm{F},j}$ is the resilience and F_j is the cover of forest in a sink cell j. m_{ij}^{k} is the moisture flow (mm) from i to j after k re-evapotranspiration events. We ranked all Amazonian 0.25° cells by their T_{weighted} values.

Dry-season intensity and seasonality. As a measure of dry-season intensity, we calculated the monthly cumulative water deficit (CWD) as the cumulative monthly evapotranspiration – rainfall, where CWD was set to 0 when rainfall exceeded evapotranspiration for a given month[18]. The mean annual water deficit at each location is the multi-year average of the annual maximum CWDs. In addition, we calculated Markham's seasonality index (MSI)—a measure of rainfall seasonality that is independent of mean rainfall. Instead, it captures the distribution of rainfall over the months of the year, whereby MSI = 100% indicates that all rainfall occurs within one month and MSI = 0% indicates that rainfall is equally distributed over the months. See ref. [75] for details.

Deforestation scenario. We also ran our simulations for 2003–2014 excluding projected deforestation up to 2050. Here, we kept all else equal. We took the cumulative deforestation from the business-as-usual deforestation scenario in an earlier study[76] (scenario C2) on 25 km resolution. Each of our 0.25° cells was assigned the deforestation value of its nearest neighbour in the dataset of ref. [76]. We show the estimated tree cover for 2050 in Supplementary Fig. 12.

Data availability. The PCR-GLOBWB hydrological model experiment uses land-cover fractions based on previous studies[21,57,77–80], as described in ref. [29]. The model was forced with WATCH Forcing Data ERA-Interim data[38] available for download at ftp://ftp.iiasa.ac.at/. The moisture-tracking model used ERA-Interim data[61] available for download at http://apps.ecmwf.int/datasets/data/interim-full-daily/ and GLDAS2 data[62] available for download at https://disc.sci.gsfc.nasa.gov/datasets?keywords=GLDAS. MODIS tree-cover data[73] are available for download at http://glcf.umd.edu/research/portal/nasaaccess2011/vcf_index.shtml, Climate Research Unit rainfall data[74] are available at https://crudata.uea.ac.uk/cru/data/hrg/, PRODES historical deforestation data are available at http://www.dpi.inpe.br/prodesdigital/prodes.php, the deforestation scenario[76] is available at http://luccme.ccst.inpe.br/en/scenarios-amazon-2050/, LandFlux-EVAL data[67] are available at http://www.iac.ethz.ch/group/land-climate-dynamics/research/landflux-eval.html, and European Space Agency GlobCover data are available at http://due.esrin.esa.int/page_globcover.php. The data that support the findings of this study are available from the corresponding author upon request.

References

52. Fittkau, E. J. Esboço de uma divisao ecológica da regiao amazônica. In *Proc. Symp. Biol. Trop. Amaz., Florencia y Leticia, 1969* 363–372 (1971).
53. Quesada, C. A. et al. Soils of Amazonia with particular reference to the RAINFOR sites. *Biogeosciences* **8**, 1415–1440 (2011).
54. Markewitz, D., Devine, S., Davidson, E. A., Brando, P. & Nepstad, D. C. Soil moisture depletion under simulated drought in the Amazon: impacts on deep root uptake. *New Phytol.* **187**, 592–607 (2010).
55. Hagemann, S. & Gates, L. D. Improving a subgrid runoff parameterization scheme for climate models by the use of high resolution data derived from satellite observations. *Clim. Dyn.* **21**, 349–359 (2003).

56. Wada, Y., Wisser, D. & Bierkens, M. Global modeling of withdrawal, allocation and consumptive use of surface water and groundwater resources. *Earth Syst. Dynam.* **5**, 15–40 (2014).
57. Hagemann S., Botzet M., Dümenil L., Machenhauer B. *Derivation of Global GCM Boundary Conditions from 1 km Land Use Satellite Data* MPI Report No. 289 (Max Planck Institute for Meteorology, 1999).
58. Weedon, G. P. et al. The WFDEI meteorological forcing data set: WATCH Forcing Data methodology applied to ERA-Interim reanalysis data. *Water Resour. Res.* **50**, 7505–7514 (2014).
59. Allen, R. G., Pereira, L. S., Raes, D. & Smith, M. *Crop Evapotranspiration—Guidelines for Computing Crop Water Requirements—Irrigation and Drainage Paper 56* (FAO, 1998).
60. Araújo A. C., von Randow C. & Restrepo-Coupe N. in *Interactions Between Biosphere, Atmosphere and Human Land Use in the Amazon Basin* (eds Nagy L., Forsberg B. R. & Artaxo P.) 149–169 (Springer, Berlin, 2016).
61. Dee, D. P. et al. The ERA-Interim reanalysis: configuration and performance of the data assimilation system. *Q. J. R. Meteorol. Soc.* **137**, 553–597 (2011).
62. Rodell, M. et al. The global land data assimilation system. *Bull. Am. Meteorol. Soc.* **85**, 381–394 (2004).
63. Lawrence, D. & Vandecar, K. Effects of tropical deforestation on climate and agriculture. *Nat. Clim. Change* **5**, 27–36 (2015).
64. Boers, N., Marwan, N., Barbosa, H. M. J. & Kurths, J. A deforestation-induced tipping point for the South American monsoon system. *Sci. Rep.* **7**, 41489 (2017).
65. Freitas, S. R. et al. A convective kinematic trajectory technique for low-resolution atmospheric models. *J. Geophys. Res. Atmos.* **105**, 24375–24386 (2000).
66. Van der Ent, R. J., Tuinenburg, O. A., Knoche, H. R., Kunstmann, H. & Savenije, H. H. G. Should we use a simple or complex model for moisture recycling and atmospheric moisture tracking? *Hydrol. Earth Syst. Sci.* **17**, 4869–4884 (2013).
67. Mueller, B. et al. Benchmark products for land evapotranspiration: LandFlux-EVAL multi-data set synthesis. *Hydrol. Earth Syst. Sci.* **17**, 3707–3720 (2013).
68. Brubaker, K. L., Entekhabi, D. & Eagleson, P. S. Estimation of continental precipitation recycling. *J. Clim.* **6**, 1077–1089 (1993).
69. Bosilovich, M. G. & Chern, J.-D. Simulation of water sources and precipitation recycling for the MacKenzie, Mississippi, and Amazon River basins. *J. Hydrometeorol.* **7**, 312–329 (2006).
70. Costa, M. H. & Foley, J. A. Trends in the hydrologic cycle of the Amazon basin. *J. Geophys. Res. Atmos.* **104**, 14189–14198 (1999).
71. Trenberth, K. E. Atmospheric moisture recycling: role of advection and local evaporation. *J. Clim.* **12**, 1368–1381 (1999).
72. Livina, V. N., Kwasniok, F. & Lenton, T. M. Potential analysis reveals changing number of climate states during the last 60 kyr. *Clim. Past.* **6**, 77–82 (2010).
73. DiMiceli, C. M. et al. *Annual Global Automated MODIS Vegetation Continuous Fields (MOD44B) at 250 m Spatial Resolution for Data Years Beginning Day 65, 2000–2010, Collection 5 Percent Tree Cover* (University of Maryland, 2011).
74. Mitchell, T. D. & Jones, P. D. An improved method of constructing a database of monthly climate observations and associated high-resolution grids. *Int. J. Climatol.* **25**, 693–712 (2005).
75. Markham, C. G. Seasonality of precipitation in the United States. *Ann. Assoc. Am. Geogr.* **60**, 593–597 (1970).
76. Aguiar, A. P. D. et al. Land use change emission scenarios: anticipating a forest transition process in the Brazilian Amazon. *Glob. Change Biol.* **22**, 1821–1840 (2016).
77. Hurtt, G. C. et al. Harmonization of land-use scenarios for the period 1500–2100: 600 years of global gridded annual land-use transitions, wood harvest, and resulting secondary lands. *Clim. Change* **109**, 117–161 (2011).
78. Olson J. S. *Global Ecosystem Framework—Definitions* (USGS EROS Data Center, 1994).
79. Olson J. S. *Global Ecosystem Framework—Translation Strategy* (USGS EROS Data Center, 1994).
80. Portmann, F. T., Siebert, S. & Döll, P. MIRCA2000—global monthly irrigated and rainfed crop areas around the year 2000: a new high-resolution data set for agricultural and hydrological modeling. *Glob. Biogeochem. Cycles* **24**, GB1011 (2010).